Transportation Research Part C 18 (2010) 536–553

Contents lists available at ScienceDirect

Transportation Research Part C

journal homepage: www.elsevier.com/locate/trc

Sensory system for obstacle detection on high-speed lines

J. Jesús García [a,*], Jesús Ureña [a], Manuel Mazo [a], Felipe Espinosa [a], Álvaro Hernández [a], Cristina Losada [a], Ana Jiménez [a], Carlos De Marziani [b], Fernando Álvarez [c], Enrique García [a]

[a] Electronics Department, University of Alcalá, Polytechnics School, Ctra. Madrid-Barcelona, km 33,700, 28805 Alcalá de Henares, Madrid, Spain
[b] Electronics Department, National University of Patagonia San Juan Bosco 9005, Comodoro-Rivadavia, Argentina
[c] Department of Electrical Eng., Electronics and Automatics, University of Extremadura, E-06071 Badajoz, Spain

ARTICLE INFO

Article history:
Received 25 July 2008
Received in revised form 8 October 2009
Accepted 12 October 2009

Keywords:
Railway safety
Obstacle detection
Infrared barrier
Efficient encoding scheme
Principal Component Analysis

ABSTRACT

This work presents an intelligent system which allows the detection of obstacles on railways. The sensory system is based on one barrier of infrared emitters and another of receivers, placed on opposing sides of the railway. Obstacle detection is achieved by a lack of reception in the detectors. The efficiency of the system is improved with the geometrical distribution of the sensory system and the encoding used at the emitting and receiving stages. Additionally optimal estimation techniques have been proposed to avoid false alarms, based on Kalman and H_∞ filtering. Furthermore, Principal Component Analysis is applied to validate the obstacle detection, and to improve the efficiency of the system. A high reliability under adverse conditions is obtained with the barrier, it now being possible to detect the presence of obstacles, and to report on their position.

1. Introduction

Since the invention of the steam engine by James Watt in 1765, its application to the first locomotive by Richard Trevithick in 1803, until the construction of the first high-speed line in 1981 between Paris and Lyon, the history of the railway (García-Márquez, 2004) was and continues to be characterized by unceasing technological advance.

In Spain, high-speed lines had an uncertain beginning with the Madrid-Seville line in 1992. But more than 15 years later, the Spanish railway is experiencing a spectacular revival. Fig. 1 shows the current high-speed lines and the ambitious project which is expected to be completed by 2020 (de Fomento, 2005). The speeds at which a train must travel to be considered as "high-speed" vary from country to country, ranging from 160 km/h to over 300 km/h. The European Union considers high-speed lines to be those at which speeds can be higher than 200 km/h. In Spain, passenger lines are being designed to permit a top speed of 350 km/h.

In all transport systems, especially in the case of the railway, there are two important concepts: safety (Reitman, 1993; Fenner, 2002; Arai, 2003) and reliability (European Directive, 2001). Because of the ever constant need to improve railway safety, several European research projects (Bon and Cassir, 2004) are carrying out research into whatever circumstances that exist which may pose a threat to railway safety. One such circumstance has received particular attention in the case of some of these projects (REOST, 2004): the existence of objects on the tracks.

In high-speed lines, zones close to bridges are considered to be quite critical, since obstacles can easily fall onto the track. This can be caused by the fall of a vehicle, or material being transported by a vehicle, onto the line. Landslides can also

* Corresponding author. Tel.: +34 918856549; fax: +34 918856591.
E-mail addresses: jesus@depeca.uah.es, jjesus.garcia@uah.es (J.J. García), urena@depeca.uah.es (J. Ureña), mazo@depeca.uah.es (M. Mazo), espinosa@depeca.uah.es (F. Espinosa), alvaro@depeca.uah.es (Á. Hernández), losada@depeca.uah.es (C. Losada), ajimenez@depeca.uah.es (A. Jiménez), marziani@depeca.uah.es (C.D. Marziani), fafranco@unex.es (F. Álvarez), enrique.garcia@depeca.uah.es (E. García).

0968-090X/$ - see front matter © 2009 Elsevier Ltd. All rights reserved.
doi:10.1016/j.trc.2009.10.002

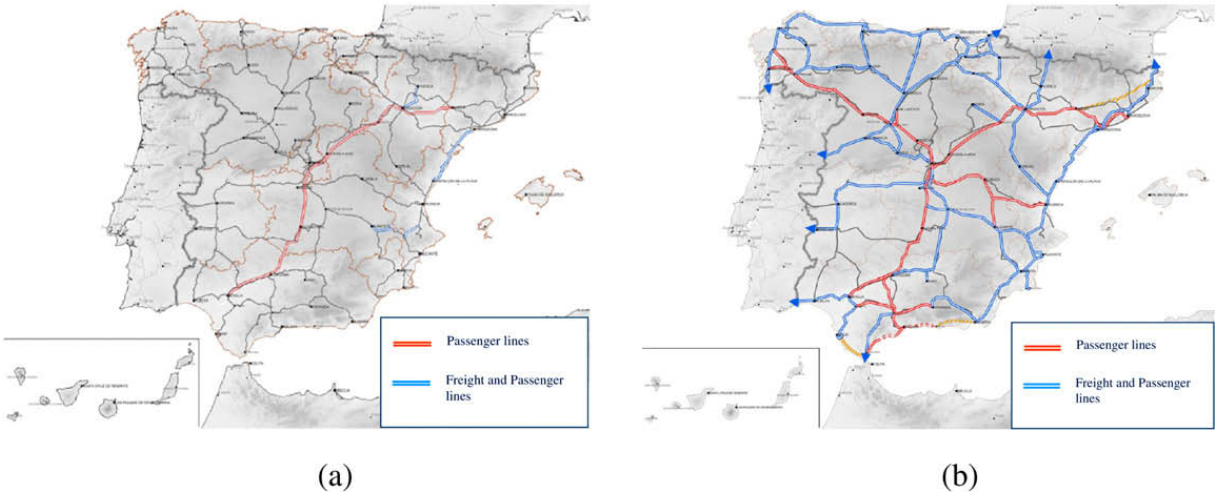

Fig. 1. Spanish high-speed lines: (a) year 2005 and (b) plan for the year 2020.

Fig. 2. Critical zones: (a) tunnel and (b) overpass.

happen at the entrances and exits of tunnels. In these critical areas, if there is a system to detect the presence of obstacles, railway traffic can be halted and possible accidents avoided.

According to Spanish Railway Regulations (GIF, 2001), a system is required to detect obstacles in such areas in the high-speed lines (see Fig. 2). This system, called *Object Fall Detector*, analyses if those zones are free of objects so that railway traffic may pass unhindered. Given the considerable growth and the expected development of the Spanish high-speed lines, the pressing need to carry out research into this area is becoming ever clearer.

In these critical areas, systems are usually placed to detect the presence of obstacles (Laseroptronix, 2005; Smartmicro, 2005), so that reports can be made to the control system. In this way, railway traffic can be halted and possible accidents avoided. However such detection systems also present the problem of generating false alarms, thus creating financial losses whenever the system detects an obstacle which does not, in reality, exist. A first solution to avoid false alarms was presented in (Garcia et al., 2005a). Here, optimal estimation techniques based on Kalman Filter and $H\infty$ filtering have been tested in order to reduce false alarms.

Regarding this problem, the rest of the paper is organized as follows: Section 2 introduces the sensory system and its geometric disposition; Section 3 deals with the emission encoding of the selected sensor to provide the system with a high immunity to noise; Section 4 analyses the typical false alarms that can affect this sensory system and presents some proposals to avoid them; Section 5 deals with the process of validating the existence of obstacle; Section 6 describes the obstacle location inside the detection area; Section 7 shows the prototype of the barrier that has been carried out and some real test; and finally, some conclusions are discussed in Section 8.

2. Sensory system and geometric distribution

2.1. Sensory system

For the application described in the previous section, the trend is the use of optical sensors, either infrared or laser (Laseroptronix, 2005). Irrespective of the sensor type chosen, all the details that will be discussed below can be applied to both types. The choice of the system may depend on financial considerations. In this work, the results shown below have been obtained using infrared emitters, mainly because this kind of sensor was required by Spanish Regulations (GIF, 2004).

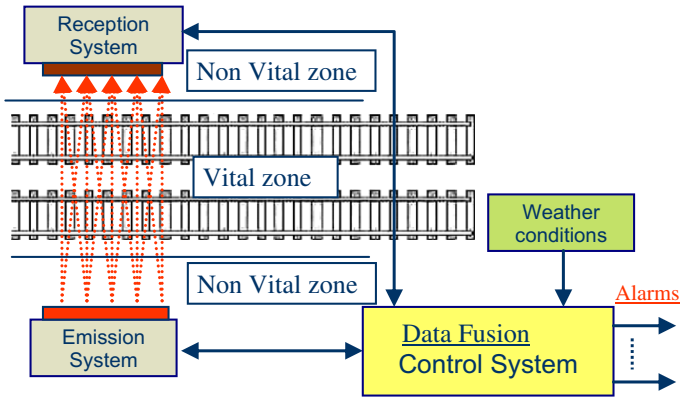

Fig. 3. Infrared barrier, placed on a section of track.

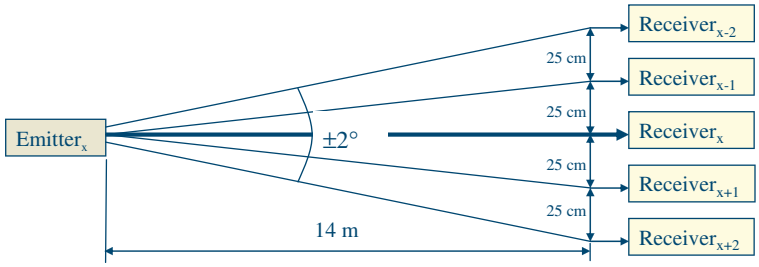

Fig. 4. Emitter–receivers links.

Infrared barriers usually consist of emitter–receiver pairs, each placed on opposing sides of the line, so it is only possible to detect the presence of an obstacle, but not its exact position. In order to detect obstacles on the railway, and distinguish at least vital areas (on the track) from the non-vital areas (outside of the track), a special structure has been designed. In this case, every emission is detected by several receivers, providing different optical links among the emitters and the receivers as is shown in Fig. 3.

The distance between emitting sensors is 25 cm, in order to successfully detect $0.5 \times 0.5 \times 0.5$ m obstacles successfully (the size is determined by railway regulations) (GIF, 2001). The configured distance between emitters and receivers is 14 m in a high-speed line. Basically, the method of obstacle detection, and its location on the railway, is based on the lack of reception by detectors. According to (GIF, 2001) the time scan of the system is 500 ms, and if an obstacle is inside the detection area more than 3 s, an alarm should be generated. For a more detailed study about the sensory system see (García et al., 2004).

2.2. Geometric distribution

Taking into account the infrared emitter beam angle ($\approx \pm 2^\circ$), if the range is 14 m, every emission reaches five receivers, as Fig. 4 shows; and reciprocally, every receiver has to detect five emissions. Fig. 5 shows the distribution of sensors in the barrier, displaying the five links that every emitter provides. For the proposed geometric distribution, the minimum emitter beam angle has to be $\pm 2^\circ$.

Regarding the distribution of the sensors, it is necessary to use five different codes to distinguish every emission in a receiver. In order to simplify the emission encoding, it has been proposed to carry out a sequential emission, by repeating the emitted codes, but at different time instant, as Fig. 5 shows. In this case, only three different codes are required. Every emitter is identified by $E^C_{x,t}$, where x is the longitudinal position in the barrier; C is the code used in the emission: R, B or G (Red[1], Blue or Green); and t is the emission time, $t1$ or $t2$. Every receiver is identified by R_x.

The emissions that can be detected on a receiver x are divided in two groups: the main and the secondary. The main group is composed of the emissions from positions x, $x-2$ and $x+2$, and this group emits at instant $t1$. The emissions from the positions $x-1$ and $x+1$ belong to the secondary group, and this group emits at $t2$. This assignment is shown in Fig. 6. The five links are used to evaluate if there are obstacles in the supervised area. If only the main group links are considered, the supervised area can be divided in three zones: on the tracks (zone 2), or outside of the tracks (zones 1 and 3), as Fig. 7 shows.

[1] For interpretation of color in Fig. 5, the reader is referred to the web version of this article.

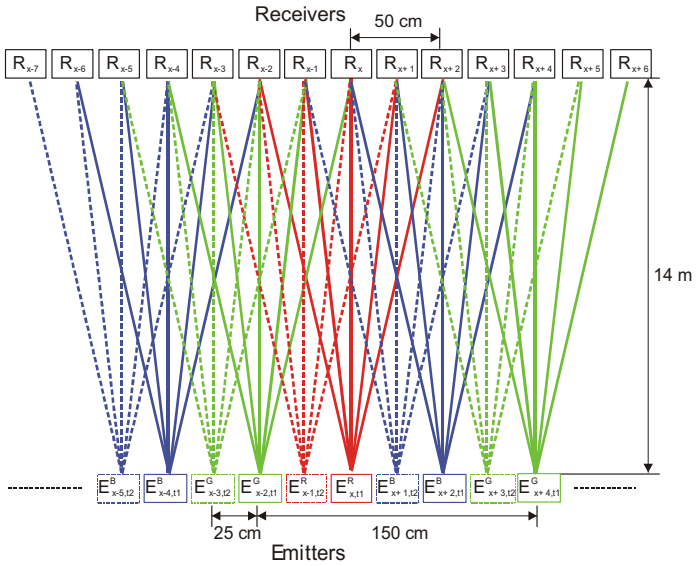

Fig. 5. Distribution of emitters and receivers.

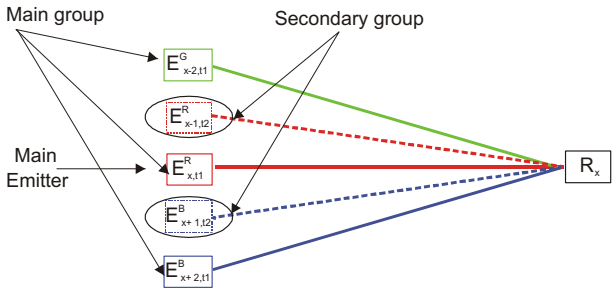

Fig. 6. Emission groups on a receiver.

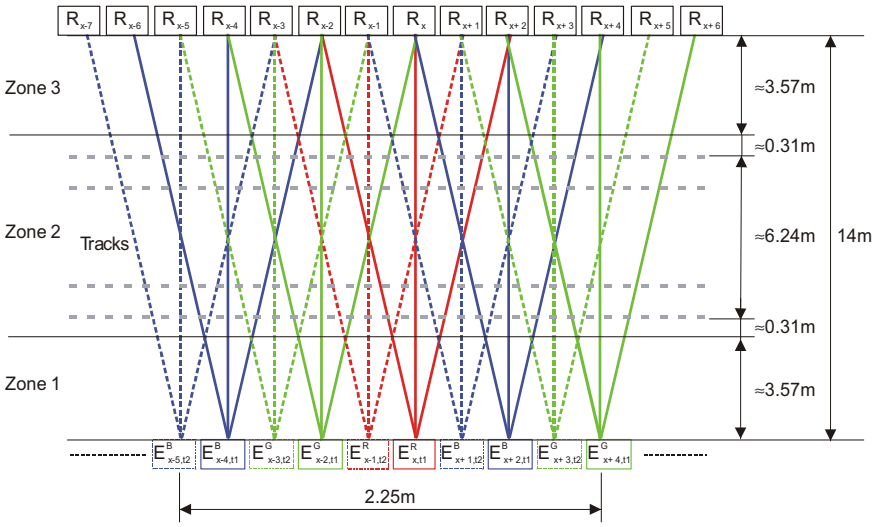

Fig. 7. Transverse supervised zones.

There are some improvements with the structure described above. On the one hand, if there is a minimum dimension obstacle in the supervised area, at least ten links are interrupted. In (GIF, 2001, 2004) only two interrupted links are required to detect the obstacle. On the other hand, due to the fact that detection is based on link interruption, if a sensor is not working, it can be mistaken for obstacle detection. The number of interrupted links allows the system to distinguish the presence

of an obstacle from an out-of-order sensor, being of particular advantage to those carrying out maintenance tasks. Finally, with this structure, obstacles can be located with this structure in two main zones: on the tracks or outside of the tracks.

3. Emission encoding

The emissions are continuously carried out by the sensors; and when the receivers do not detect some of the emissions, the presence of an obstacle can be concluded. According to the geometry of the system shown in Fig. 7, the radiation coming from three emitters could be received by every receiver at the same time instant. In order to discriminate the source of these emissions, it is necessary to encode them. To avoid interferences among the three codes, mutually orthogonal (MO) sets of sequences have been used. For a more detailed discussion about MO sets of sequences, see (Tseng and Liu, 1972; Shu-Ming and Bell, 2000).

A complementary set of sequences (CSS) is a set of binary sequences whose elements are either +1 or −1, having the property that the sum of their aperiodic auto-correlation functions is zero for all nonzero time-shifts. In particular, if $\{a, b, c, d\}$ is a set of four sequences (Álvarez et al., 2004) with length L, and φ_{xx} represents the auto-correlation function of the sequence $x(k)$ then:

$$\phi_{aa}(k) + \phi_{bb}(k) + \phi_{cc}(k) + \phi_{dd}(k) = \begin{cases} 4L, & \text{if } k = 0 \\ 0, & \text{otherwise} \end{cases} \tag{1}$$

Given two sets $\{a_1, b_1, c_1, d_1\}$ and $\{a_2, b_2, c_2, d_2\}$, both are orthogonal if the addition of the cross-correlation function of the sequences of each set is zero. If φ_{xy} represents the cross-correlation function of the sequences $x(k)$ and $y(k)$ then:

$$\phi_{a_1a_2}(k) + \phi_{b_1b_2}(k) + \phi_{c_1c_2}(k) + \phi_{d_1d_2}(k) = 0 \quad \forall k \tag{2}$$

The set of complementary sequences used in the emitter, not only discriminates the source of the emission, but also provides a high noise immunity to the system, as the obtained results show. Although four mutually orthogonal sets of four sequences can be obtained, in the application described only three sets are required since it is only necessary to distinguish three emissions. Fig. 8 shows the emission with four emitters and one receiver. The emitter and receiver units are synchronized, mainly for safety reasons.

In Fig. 8, every emitter i transmits the set $\{a_i, b_i, c_i, d_i\}$ continuously, by interleaving the bits of the sequences (the set length is $4L$). Its continuous emission allows a signal to be obtained in the detector with period $4L$ and a maximum peak of $4L$, thus showing that there is not an obstacle between the emitter and the receiver, according to Eq. (3). The index i means any emission in the system, $i = 1, 2, 3$, or 4.

$$\text{Detector\_output}_i = z_i(k) = 4L \sum_{j=0}^{j=\infty} \delta(k - j \cdot 4 \cdot L) \tag{3}$$

Fig. 9 shows the results when using 256-bit sequences ($L = 256$), with a SNR of −6 dB. The continuous emission provokes a periodical detector output, as Eq. (3) shows. If an obstacle is detected in front of a receiver, the peaks shown in Fig. 9 disappear, the output being null while the obstacle is on the railway. The peak detector threshold is fixed at $2L = 512$, and the maximum correlation output can be 1024 ($4L$).

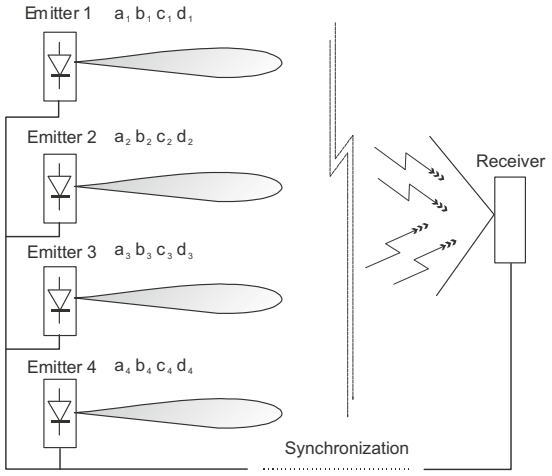

Fig. 8. Detail of the four emitters and the receiver.

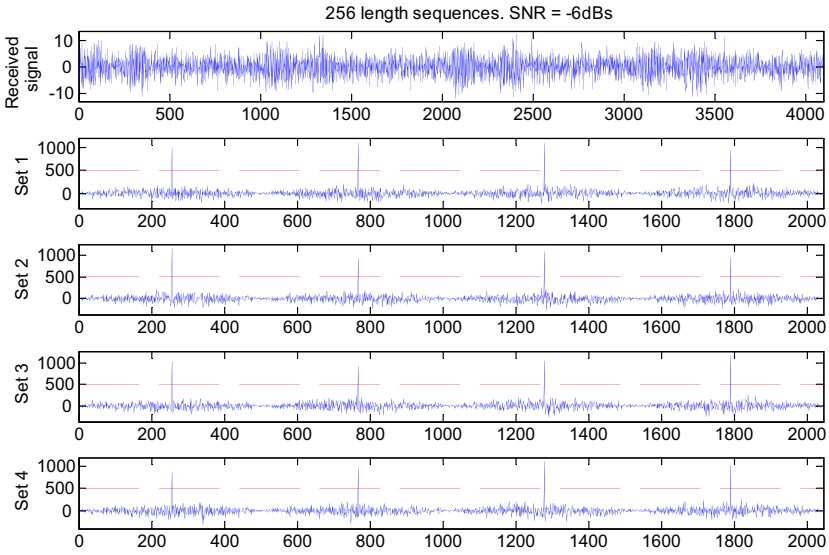

Fig. 9. Detector output for every emission ($L = 256$, SNR = -6 dB).

4. False alarms discrimination

The outdoor infrared system suffers from diverse losses and disturbances, which can produce an erroneous detection. If the receiver does not detect one emission during a predefined time, an alarm will be generated, thus concluding that there is an obstacle on the railway. But if the obstacle does not exist, the alarm is actually false. As far as possible, it is necessary to avoid the generation of false alarms, and as a result, they have to be discriminated. In this work it is proposed to use optimal estimation techniques to reduce false alarms.

4.1. False alarms generation

In these outdoor optical systems there are some phenomena that can provoke false alarms, mainly weather conditions and the solar radiation. There are other reasons, such as propagation losses or wrong alignment of emitters and receivers. We assume that the latter have been already considered in the link design.

4.1.1. Atmospheric attenuation

Snow, fog, and rain are considered. Although there are numerous studies about the losses due to meteorological conditions, the Eq. (4) shown below is used to quantify them (Kim et al., 1998).

$$L_{atm}(dB) = \frac{13}{V} \cdot R \tag{4}$$

where V is the visibility and R is the link range, they both in kilometers. Table 1 shows the relation between weather conditions and visibility.

If the attenuation defined in Eq. (4) is very strong, the correlation peak might not be high enough, and the system could consider that an obstacle exists.

4.1.2. Solar interference

As the photodiode wavelength (850 nm) is inside the solar spectrum, natural background light can potentially interfere with signal reception. The solar effect on the IR barrier is photodiode saturation (Bloom et al., 2003). It implies that the sequence detection does not work, providing a lack of reception as if there was an obstacle.

The following subsections show two proposals to reduce false alarms due to atmospheric attenuation or solar radiation.

Table 1
Relation between visibility and weather conditions.

Visibility (V)	Weather conditions
$V > 50$ km	Very clear
6 km $< V <$ 50 km	Clear
1 km $< V <$ 6 km	Haze/snow/light rain
0.5 km $< V <$ 1 km	Light fog/snow/heavy rain
$V < 0.5$ km	Thick fog

4.2. False alarms discrimination using the Kalman Filter

When there are neither obstacles on the railway nor false alarms, the correlation outputs are the same as shown in Fig. 9. In this situation, when there is a lack of signal due to weather conditions or solar interference, false alarms can be produced. To avoid this, in (Garcia et al., 2005a) the use of a dynamic threshold for the peak detector was proposed, where every correlation output was estimated by polynomial interpolation of degree 1, and the estimated output was used to dynamically change the threshold. But as was shown in (Garcia et al., 2005a), whilst the false alarms were reduced, they were not completely eliminated.

To improve the system, Kalman Filter (KF) is proposed to estimate the system output, and to obtain the dynamic threshold. Due to the fact that the system output changes according to the weather conditions, Eq. (3) will be:

$$z_k = 4 \cdot L \cdot \theta_k + \phi_{\eta_k} \tag{5}$$

where θ_k represents the atmospheric attenuation, ϕ_{η_k} the noise component (correlation between the sequences and the additive noise at the receiver), and k is the time instant when the correlation output is obtained. Taking into account Eq. (4), in a 14 m link (the distance among emitters and receivers in the obstacle detection system), the atmospheric attenuation is:

$$\theta_k = 10^{-\frac{18.2}{V_k}} \tag{6}$$

where V_k is the value of the visibility in meters in the instant k. Now, we consider a discrete-time system represented by the state and output equations:

$$\begin{aligned} \mathbf{x}_{k+1} &= \mathbf{A}\mathbf{x}_k + \mathbf{B}\mathbf{u}_k + \mathbf{w}_k \\ \mathbf{z}_k &= \mathbf{C}\mathbf{x}_k + \mathbf{v}_k \end{aligned} \tag{7}$$

where $\mathbf{x}_k$ is the state vector, and in this case $\mathbf{x_k} = \theta_k$ (the atmospheric attenuation), and $\mathbf{u}_k$ is the visibility variation $(V_k - V_{k-1})$. Here, $\mathbf{w}_k$ is the *process noise* (system disturbances, modelling errors, etc.); $\mathbf{z}_k$ the measurement vector and $\mathbf{v}_k$ is the *measurement noise*, all of appropriate dimensions. To apply the KF, it is assumed that the noise signals be of zero-mean value, that is, $E[w] = E[\mathbf{v}] = 0$. The KF for the minimum-variance estimate is given by a recursive scheme, as can be observed in (Dutton et al., 1997). In this particular case, to obtain the state equations, Eq. (6) has been linearized for a visibility of 1 km, being the result:

$$\theta_k = \theta_0 + \left.\frac{\partial\theta}{\partial V}\right|_{V_0=1\text{km}} (V_k - V_0) \tag{8}$$

And θ_{k+1} will be:

$$\theta_{k+1} = \theta_k + \left.\frac{\partial\theta}{\partial V}\right|_{V_0=1\text{km}} (V_{k+1} - V_k) \tag{9}$$

The space state representation is obtained from Eqs. (5) and (8). The following values have been considered:

$$\begin{aligned} &x_k = \theta_k \\ &u_k = V_k - V_{k-1} \\ &\mathbf{A} = 1; \quad \mathbf{C} = 4L \\ &\mathbf{B} = \left.\frac{\partial\theta}{\partial V}\right|_{V_0=1\text{km}} = \frac{18.2}{1000^2} 10^{-18.2/1000} = 1.7453 \times 10^{-5} \end{aligned} \tag{10}$$

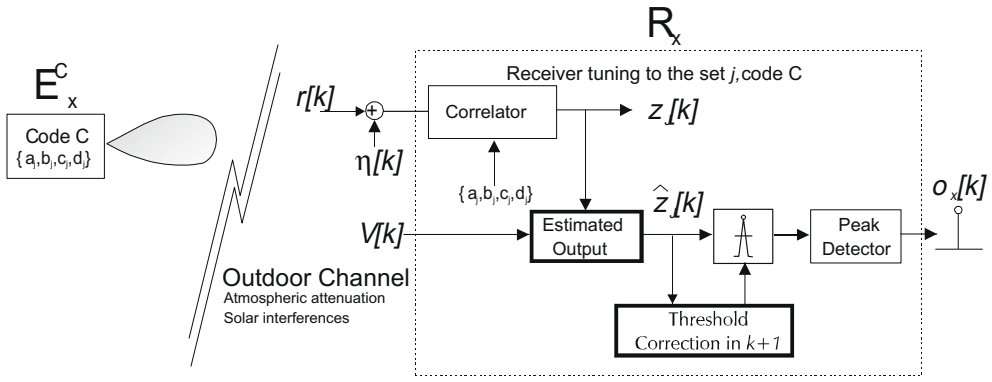

Fig. 10. Block diagram with dynamic threshold, for the detection of one emission.

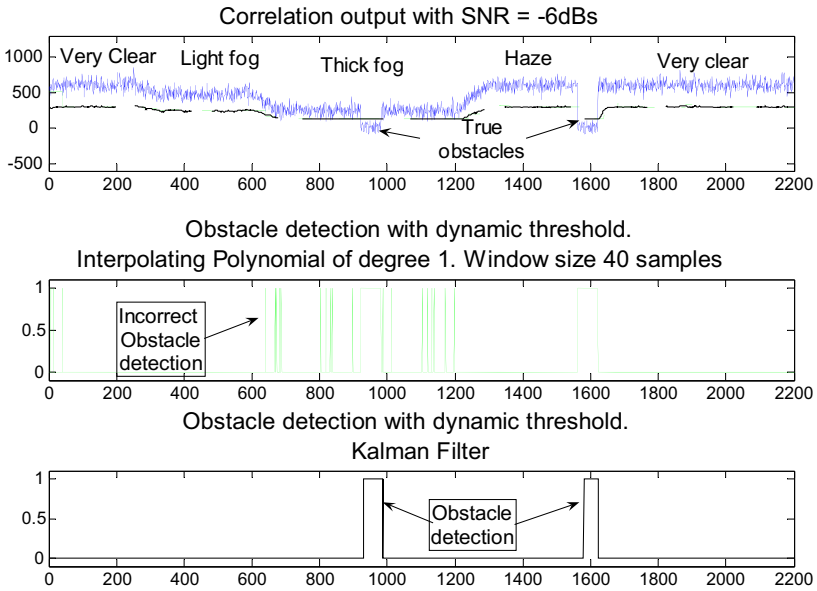

Fig. 11. Dynamic threshold evaluation in different weather conditions, using a polynomial interpolation and the Kalman filter.

Using the KF, the system output is estimated, and according to such output, the threshold in the instant k is determined to be half of the estimation at $k-1$. Fig. 10 shows a block diagram for one emitter and one receiver, both using the same code C (C can be one of sets described in Section 3), with the dynamic threshold correction. The reception block is the same for every receiver, but three codes are detected by using the same block diagram as is shown in Fig. 10. In Fig. 10, $r[k]$ is the received signal, $\eta[k]$ the additive channel noise, $z_j[k]$ the correlation output j, $V[k]$ the visibility and $o_x[k]$ the peak detector output from the receiver R_x.

The algorithm has been simulated in different weather conditions with a SNR = −6 dB. In Fig. 11, the graph at the top shows the correlation output for different weather conditions, the estimated output and the dynamic threshold calculated from the KF. The central graph shows the peak detector output, but using the dynamic threshold with the polynomial interpolation of degree 1 (Garcia et al., 2005a). The graph at the bottom shows the peak detector output ($o_x[k]$ in Fig. 10) using the dynamic threshold obtained with the KF, and in this case, all the obstacle detections are correct. We can conclude that in these conditions, the KF reduces the false alarms due to atmospheric attenuation.

Fig. 12 shows the simulation with a SNR = −6 dB and with different relative levels of sunlight, increasing with time. The higher the solar radiation is, the lower the correlation output is. In such a situation, the dynamic threshold works better with

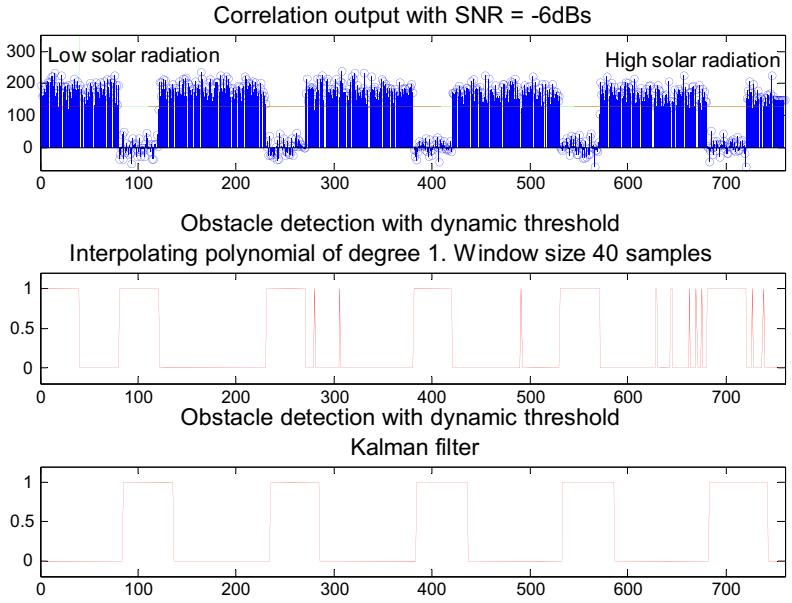

Fig. 12. Dynamic threshold evaluation with different relative levels of sunlight.

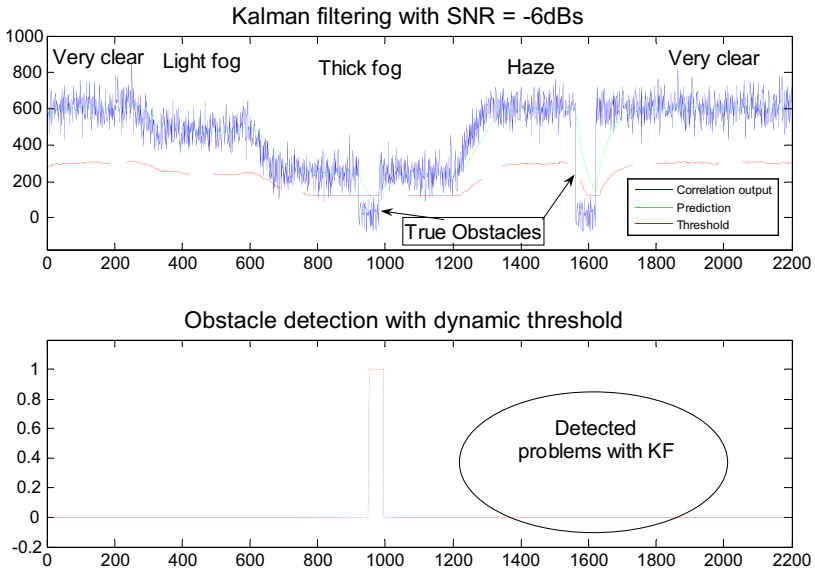

Fig. 13. Wrong obstacle detection using Kalman Filter.

the KF than the polynomial interpolation. Even though the obstacle detection with dynamic threshold using the KF is suitable for the situations illustrated above, there are a couple of serious limitations: it assumes that the channel noise statistic is known and it minimizes the average estimation error. Fig. 13 shows a situation where the noise statistical is unknown. As can be observed, obstacle detection is not always successful. In order to solve this problem, another filtering technique is proposed in next section.

4.3. False alarms discrimination using H∞ filtering

In this section the H∞ filtering, also known as *minimax* filtering (Simon, 2000, 2005), is proposed for two basic reasons: this system is based on infrared technology and it is difficult to characterize the channel noise; furthermore, due to the fact that this area of transport safety is achieved by the correct operation of the obstacle detector, it is important to minimize the worst case (and not only the average) of the estimation error. It is called *minimax* filter because it tries to minimize the maximum estimation error.

With the receiver information and with a detailed knowledge of the dynamic of the system, the $\mathbf{x}_k$ estimation (by applying H∞ criteria (Simon, 2000)), is carried out by minimizing the index:

$$J = \frac{ave\|\mathbf{x}_k - \hat{\mathbf{x}}_k\|_{\mathbf{Q}}}{ave\|\mathbf{w}_k\|_{\mathbf{W}} - ave\|\mathbf{v}_k\|_{\mathbf{V}}} \tag{11}$$

where $\|\mathbf{x}\|_{\mathbf{Q}}^2 = \mathbf{x}^T\mathbf{Q}\mathbf{x}$ and *ave* means average value.

Even in the worst case of *process noise* $\mathbf{w}_k$ and *measurement noise* $\mathbf{v}_k$, the average values are taken over all time samples k. Furthermore, $\mathbf{Q}$, $\mathbf{W}$, and $\mathbf{V}$ are diagonal matrixes that are used in the weighted norms in J and must be chosen by the designer. To make the estimation problem easier, the relation is assumed to be:

$$J < 1/\gamma \tag{12}$$

where γ is a constant number chosen by the designer. In other words, the aim is to find a state estimate so that the maximum value of J is always less than any estimation, regardless of the terms $\mathbf{w}_k$ and $\mathbf{v}_k$. Furthermore, γ has to be chosen so that all the eigenvalues of the covariance matrix of the estimation error have magnitudes less than one. In (Simon, 2000) there is a more detailed discussion about H∞ filtering. As in the case of KF, a recursive scheme is used to obtain the state estimation. The state estimate that produces $J < 1/\gamma$ is given as follows:

$$\mathbf{L}_k = [\mathbf{I} - \gamma\mathbf{Q}\mathbf{P}_k + \mathbf{C}^T\mathbf{V}^{-1}\mathbf{C}\mathbf{P}_k]^{-1} \tag{13}$$

$$\mathbf{K}_k = \mathbf{A}\mathbf{P}_k\mathbf{L}_k\mathbf{A}^T + \mathbf{W} \tag{14}$$

$$\hat{\mathbf{x}}_{k+1} = \mathbf{A}\hat{\mathbf{x}}_k + \mathbf{B}\mathbf{u}_k + \mathbf{K}_k(\mathbf{z}_k - \mathbf{C}\hat{\mathbf{x}}_k) \tag{15}$$

And the covariance matrix of the estimation error $\mathbf{P}_k$ is updated as follows:

$$\mathbf{P}_{k+1} = \mathbf{A}\mathbf{P}_k\mathbf{L}_k\mathbf{A}^T + \mathbf{W} \tag{16}$$

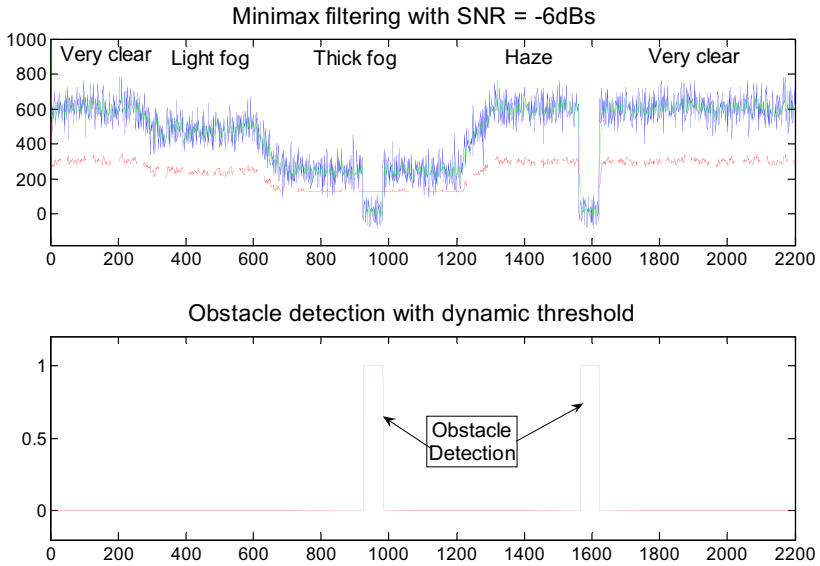

Fig. 14. Dynamic threshold evaluation in different weather conditions, using minimax filtering.

According to Eqs. (13)–(16), this filter requires more tuning in order to perform adequately. Apart from the values shown in Eq. (10), the following values have been empirically considered for the tuning parameters in H∞ filtering: $P_0 = 10{,}000$, $Q = 10$, $V = 10$, $W = 10^{-6}$, $\gamma = 500$.

Fig. 14 shows the results by applying *minimax* filtering to dynamically change the threshold, in different weather conditions, and with a SNR = −6 dB, as was shown in Fig. 13, where there was a wrong obstacle detection with the KF, but where now an obstacle is correctly detected. As it was done with the KF, the threshold in the instant k is determined to be half of the estimation at $k - 1$.

5. Validation of obstacle detection

In a railway environment, typical situations that can generate a false alarm must be identified. Although, the occurrence of false alarms has been notably reduced by using optimal filtering, it is still possible for some receivers not to detect the emission because a small object has temporarily interrupted the link. Typical sporadic cases of cuts of the links can be either leaves or small animals in movement. As well as the optimal filtering, it is proposed to use Principal Component Analysis (PCA) (Turk and Pentland, 1991), so that the above mentioned situations do not cause alarm activations. The proposal consists of jointly using both techniques, as Fig. 15 shows.

As can be seen in Fig. 15, optimal filtering is applied to every receiver. In this case, $\mathbf{z}_x$ is the correlation result without applying optimal filtering (see Fig. 10). It is a vector of five components, one for every link that is analysed in the receiver

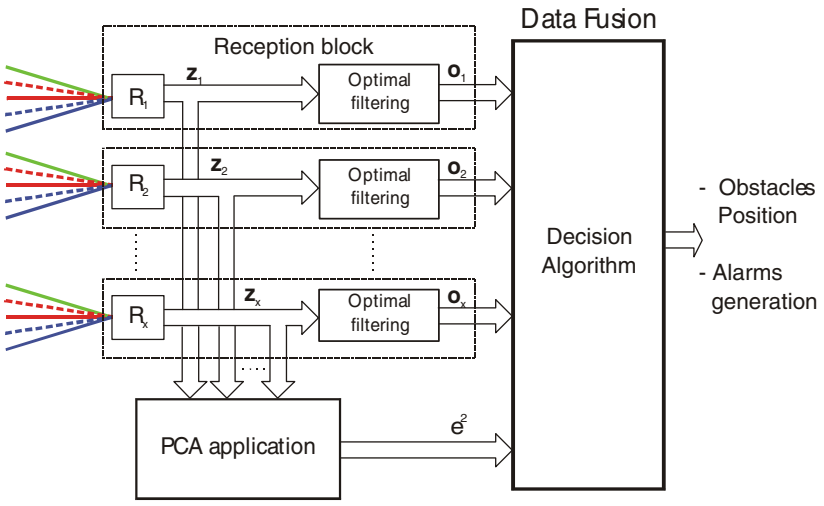

Fig. 15. Validation of obstacle detection.

R_x (see Fig. 6). $\mathbf{o}_x$ is a vector of five binary components (1 = link on, 0 = link interrupted), and it represents the peak detector output for every link. Furthermore, PCA is applied to all the correlation outputs, and it obtains global information about the existence of obstacles, no only evaluating the state of individual links. Next section deals with the use of PCA in this work. Finally, a decision algorithm has to evaluate if it is necessary to activate the alarms because one or more objects are inside the detection area.

5.1. Principal Component Analysis

In general, PCA is divided into two phases. The first one is the training process, and it is carried out *off-line*, when varying operational conditions have been taken into account (conditions of sunlight, meteorology, noise levels, etc.), with the section of track free of obstacles. In this situation a data set is captured, and it is used to obtain the transformation matrix **U** between the original space and the transformed one, or vice versa. The **U** matrix is obtained from the eigenvectors associated with the most significant eigenvalues of the covariance matrix of the data set. The second phase is *on-line*, when the sensory system is working. By using the transformation matrix **U**, the measurements that are received from the process unit (vector of measurements taken from the receivers) are projected onto the transformed space according to:

$$\mathbf{y} = \mathbf{U}^T\mathbf{s} \tag{17}$$

Later the reconstruction is computed using:

$$\hat{\mathbf{s}} = \mathbf{U}\mathbf{y} \tag{18}$$

where **s** is the vector of characteristics with zero mean, on which the transformation is carried out and **y** is the resultant vector from the transformation and represents the reconstruction vector. According to Fig. 15, **s** is obtained as follows:

$$\mathbf{s} = [\mathbf{z}_1 \quad \mathbf{z}_2 \quad \ldots \quad \mathbf{z}_x] \tag{19}$$

The reconstructed information will differ from the original in either major or minor magnitude depending on the grade of similarity that exists between the new data and those which were used to obtain the transformation matrix **U**. This difference is known as the reconstruction error ε:

$$\varepsilon^2 = \|\mathbf{s} - \hat{\mathbf{s}}\| \tag{20}$$

If the error ε is larger than a determined threshold, it is concluded that an object exists. Fig. 16 depicts the described process.

To analyse the viability of the PCA technique, the measurements from a 3 m barrier (see Fig. 5) have been processed on-line. This section of barrier is composed of 15 emitters and 12 receivers. In this situation, **s** is a 60-dimensional vector. Because the different receivers are very close, a high correlation generally exists among different components of the vectors, so that PCA notably reduces any redundant information. In order to consider the majority of the possible scenarios of detection in absence of obstacles, the information of the *off-line* process (training stage) has been obtained for different values of the SNR (from −6 dB up to 6 dB), as well as in different conditions of visibility, shown in Table 1. Fig. 17 shows the reconstruction error when the track is free of obstacles, and SNR = 0 dB. Whenever the section of track is free of obstacles, the reconstruction error takes small values.

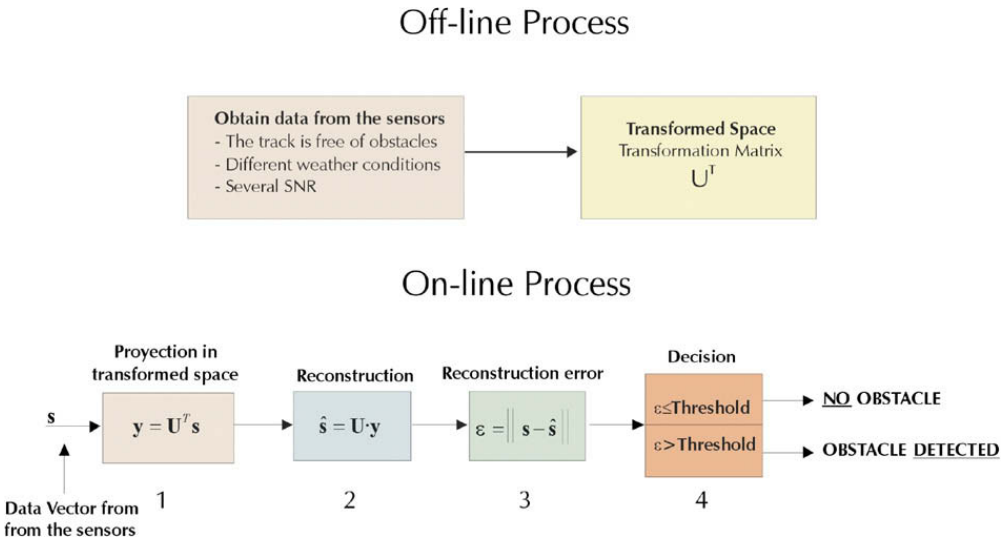

Fig. 16. PCA processes.

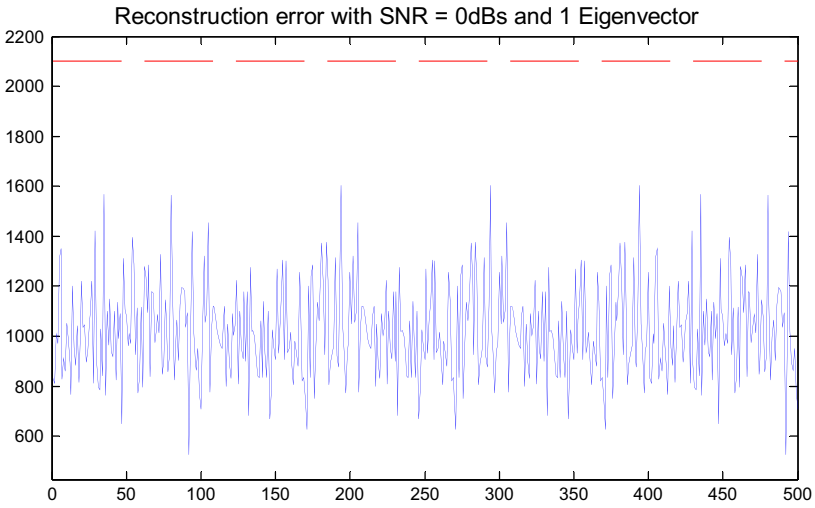

Fig. 17. Reconstruction error when the section of track is free.

Fig. 18. Reconstruction error when the section of track is not free.

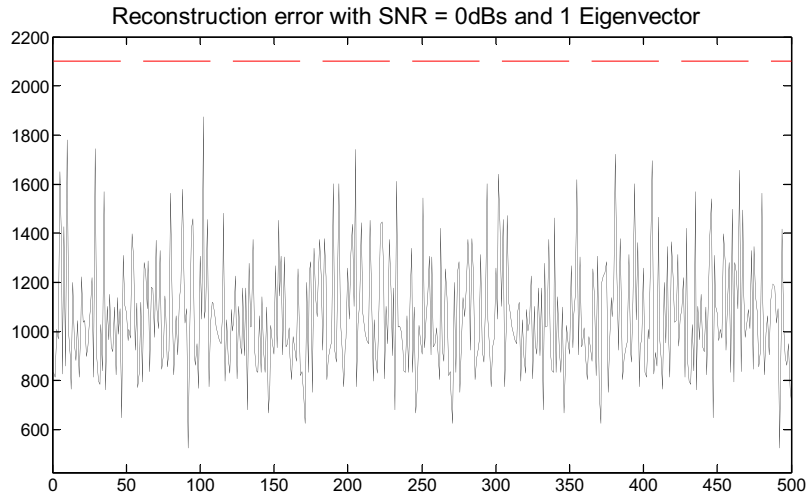

Fig. 19. Reconstruction error when there are random cuts.

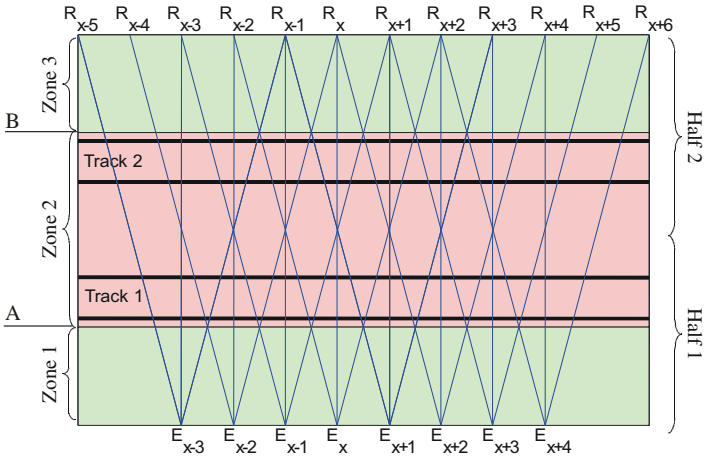

Fig. 20. Location areas.

Fig. 18 shows the reconstruction error when a pedestrian is crossing the tracks transversely. At every time instant a group of receivers detect the presence of the above mentioned obstacle. As this obstacle interrupts several links, the similarity between the spaces decreases, and the reconstruction error increases suddenly over the threshold, its value being proportional to the number of links that are interrupted by the obstacle. The reconstruction error is higher than the threshold during the time that the obstacle exists. The original covariance matrix has 60 eigenvectors, but in this case, only one eigenvector has been used in the final transformation, meaning a high reduction in redundant information.

In Fig. 19 another situation is described when there is a random lack of radiation at the receivers for a short time. Such is typical in the case of flying leaves, or the flight of birds inside the detection area. These situations are filtered by PCA because the reconstruction error is always lower than the threshold.

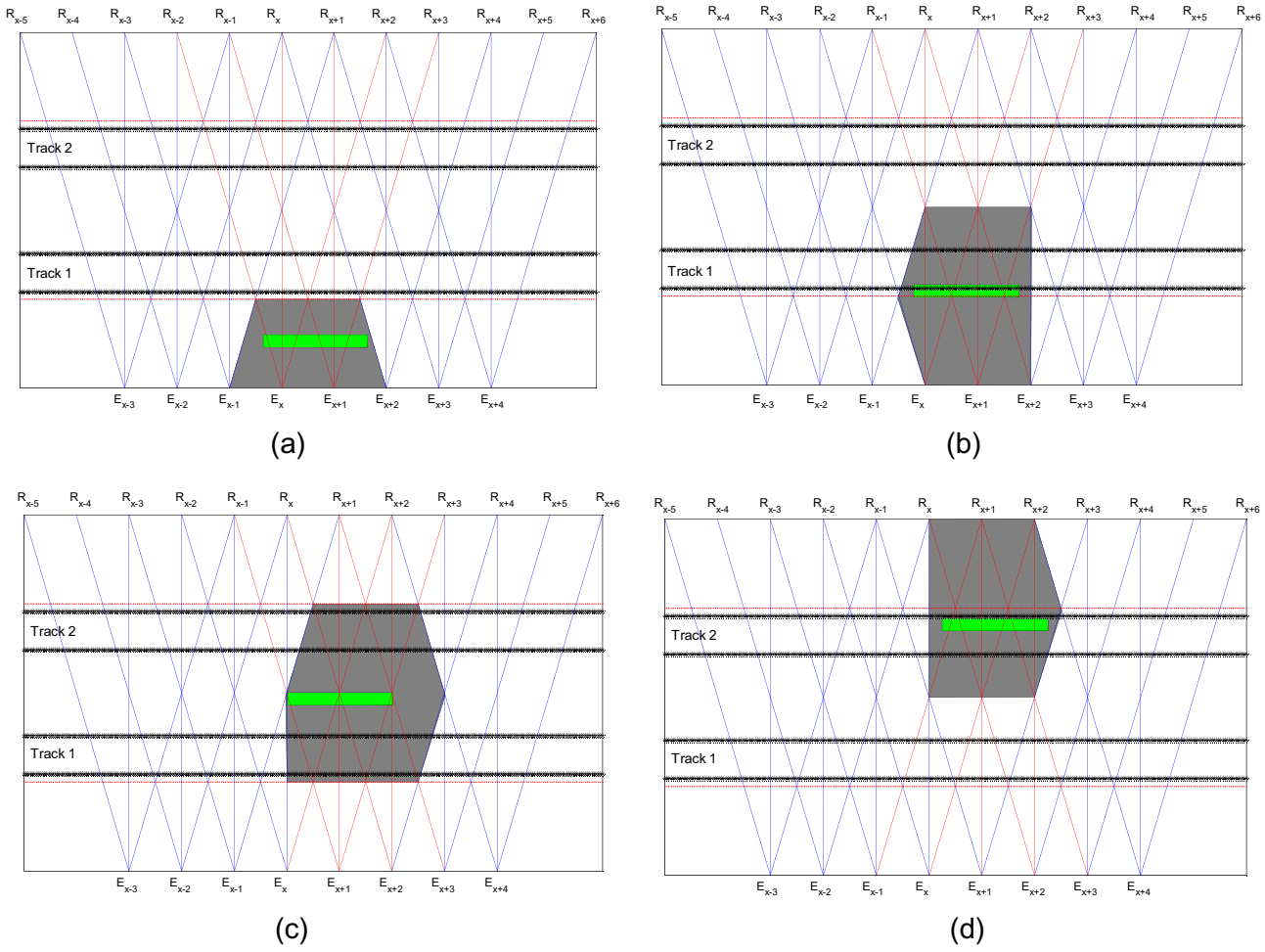

Fig. 21. Obstacle location: (a) zone 1; (b) zone 1 and 2 (half 1); (c) zone 3; and (d) zone 2 and 3 (half 2).

The PCA process is used to increase the reliability of the object detector, as a more accurate detection can be carried out for obstacles inside the supervised area. Furthermore, PCA filters the situations of random interrupted links, such as in the case of small objects entering and leaving the supervised area over a short period of time.

6. Obstacle location

Since the existence of an obstacle on the railway can be detected with high reliability, it is possible to locate it by taking advantage of the geometric distribution of the sensors. At this stage, only the digital outputs, o_x, obtained after the optimal filtering are considered (see Fig. 15).

The location algorithm obtains the longitudinal (in the track direction) and transverse position. To obtain the longitudinal one, it only is necessary to know that a lack of reception in the axial axis is occurring, between emitter and receiver. The detection area has been divided into three transverse zones, as was shown in Fig. 7. To locate the obstacle in one of these three zones, a geometrical analysis has been carried out (García et al., 2005b) according to the structure shown in Fig. 20. The obstacle can be transversely located in five positions: zone 1, zone 2, zone 3, half 1 (zones 1 and 2) and half 2 (zones 2 and 3). A program has been developed to evaluate the different locations. Fig. 21 shows some location results which validate the proposed algorithms.

7. Prototype of the barrier

To evaluate the feasibility of the proposed system and algorithms, a prototype of the barrier has been implemented (see Fig. 22). Several real tests have been performed to analyse the discrimination of false alarms and the validation of obstacle detection. For all the tests (indoor or outdoor), the distance between both barriers has been 14 m.

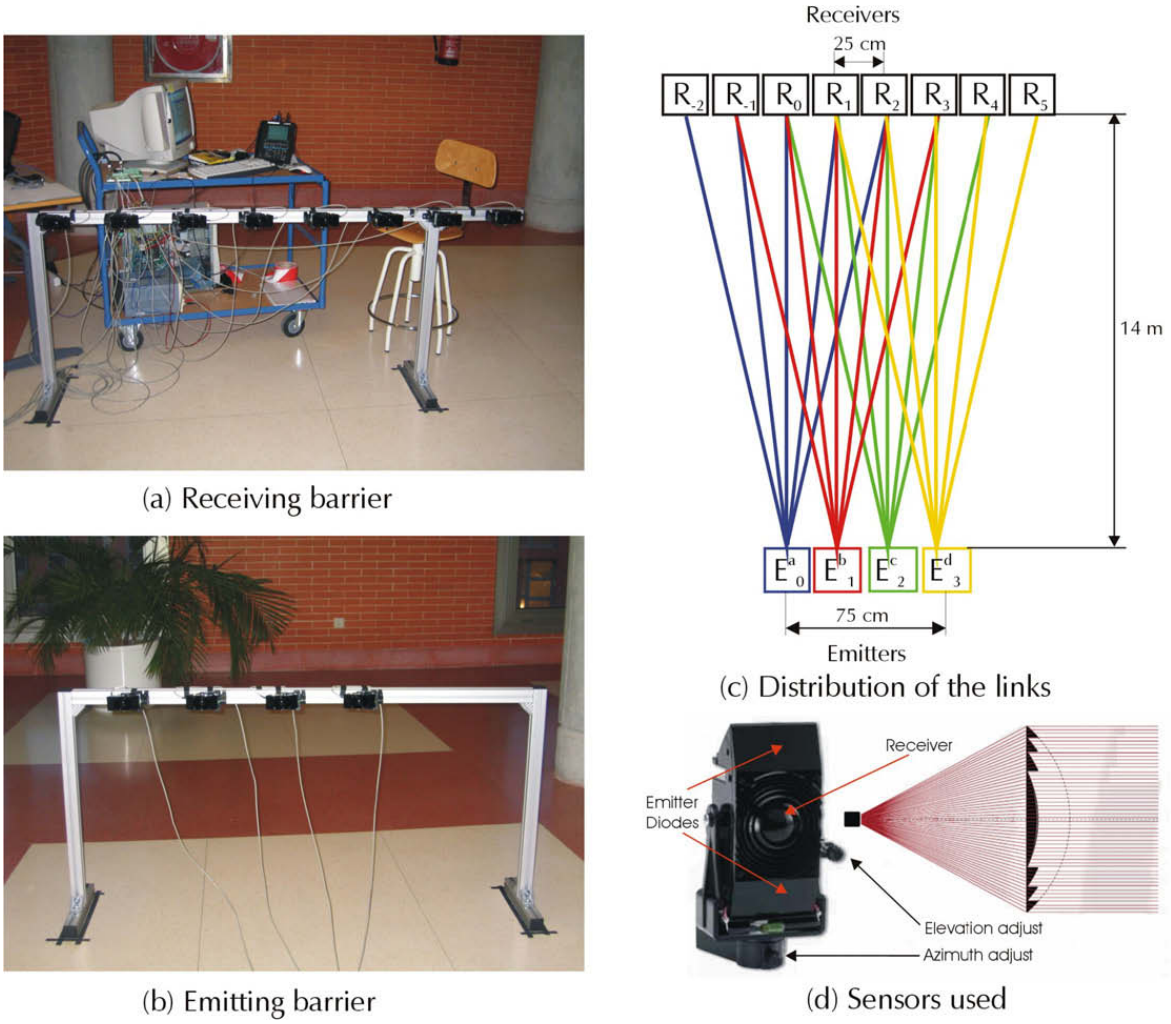

Fig. 22. Prototype of the infrared barrier: (a) receiving barrier; (b) emitting barrier; (c) distribution of the links; and (d) detail of the sensors used.

The receiving barrier is based on eight receivers (Fig. 22a) and the emitting one in four emitters (Fig. 22b). Fig. 22c also shows the established links among emitters and receivers, and Fig. 22d shows a detail of the sensor used (Sorhea, 2009). The sensor case is the same for emitters and receivers, so, the only difference is the electronic device used.

Fig. 23 shows the real multi-detection carried out in an IR receiver (receiver 1 according to Fig. 22c) in absence of obstacles, by using the encoding scheme proposed in Section 3 (see Eq. (3)). According to the encoding scheme, the maximum correlation output can be 1024, and the period of the correlation output is 102,4 ms. Considering railway regulations, the maximum scan time should be 500 ms. In that time, the prototype generates almost five measurements about the state of the tracks. In this case, the detector threshold has been fixed at 100. In Fig. 23, the amplitude differences depend on the lateral deviations between emitters and receiver (see Figs. 4 and 6), so the maximum correlation output is provided by the emitter placed in the axial axis. If one emitter is not aligned with its corresponding receiver (there exists a lateral

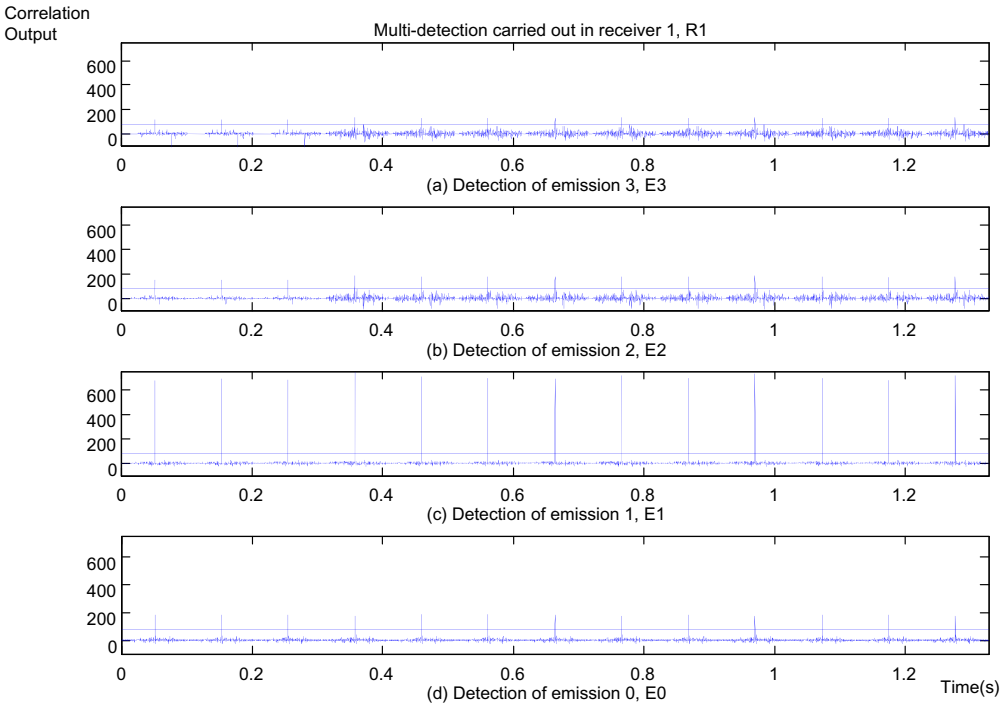

Fig. 23. Real correlation outputs obtained in IR receiver 1 when the links are not interrupted.

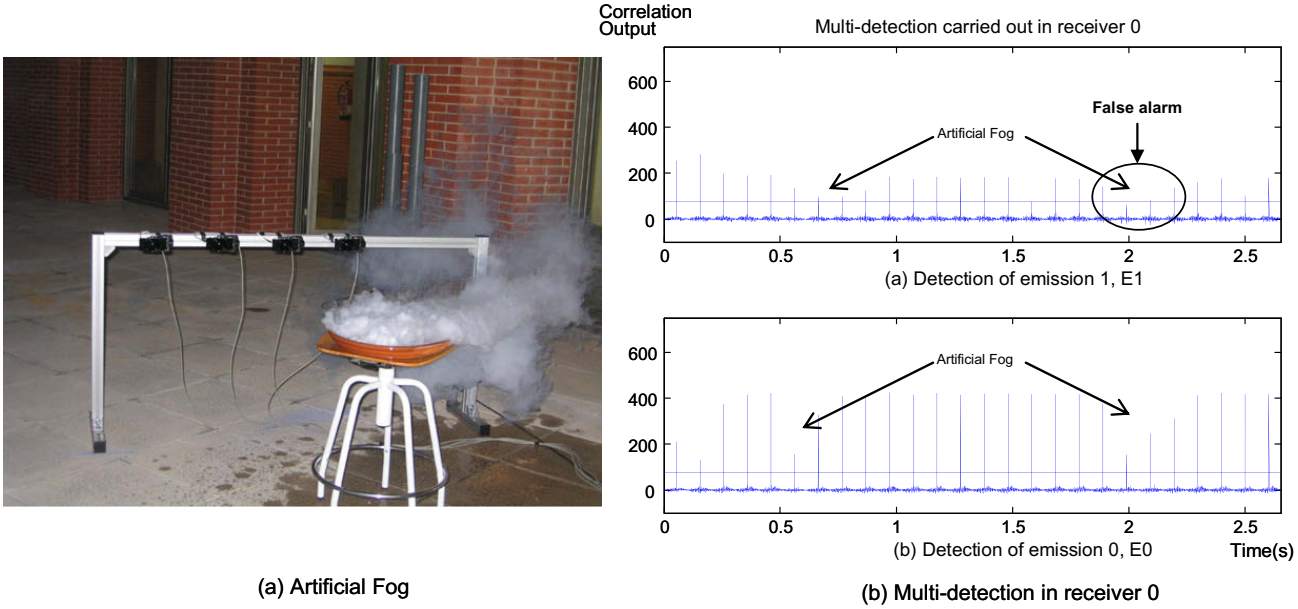

Fig. 24. Multi-detection carried out in receiver 0 when artificial fog is generated. (a) Artificial fog generation and (b) correlation outputs.

or angular deviation between them), there will be a reduction of the correlation output depending on the emission and reception patterns (Díaz et al., 2007). With the chosen sensors (Sorhea, 2009), the detection is carried out correctly even with angular deviations of ±1.5°.

Since it is difficult to test the barrier under extreme weather conditions, for the reduction of visibility, optical filters have been used to reduce the level of signal in the IR receivers and artificial fog has been created in front of the emitters. Fig. 24 shows a test where artificial fog has been generated. As can be observed, when fog exists the correlation values decrease, being even lower than the established fixed threshold. This situation could generate a false alarm, thus justifying the use of a dynamic threshold. Due to the fact that the best simulated results have been obtained by using H∞ filter, this is the only one that has been tested outdoors. The tuning parameters are the same as were described in Section 4.3. Fig. 25 shows a test where optical filters have been used. Fig. 25b depicts the estimated correlation output and how the dynamic threshold is adapted to visibility conditions. For safety reasons, the minimum value of the threshold has been fixed at 100 (the maximum correlation output can be 1024). As Fig. 25c shows, if an obstacle exists when the correlation output is lower than the minimum threshold, it is not possible to detect it. In Fig. 25c, '1' means active link, and '0' interrupted link. It is important to consider that the maximum degradation of IR links in the barrier due to the meteorology is 60% (thick fog). In some tests, to analyse the robustness of the H∞ filter, the artificial attenuation has been higher than 75%.

Finally, PCA technique has been analysed by using the prototype of the barrier. In this case, there are only 20 links (see Fig. 22c), and the vector of characteristic **s** is a 20-dimensional vector. The information of the *off-line* process has been

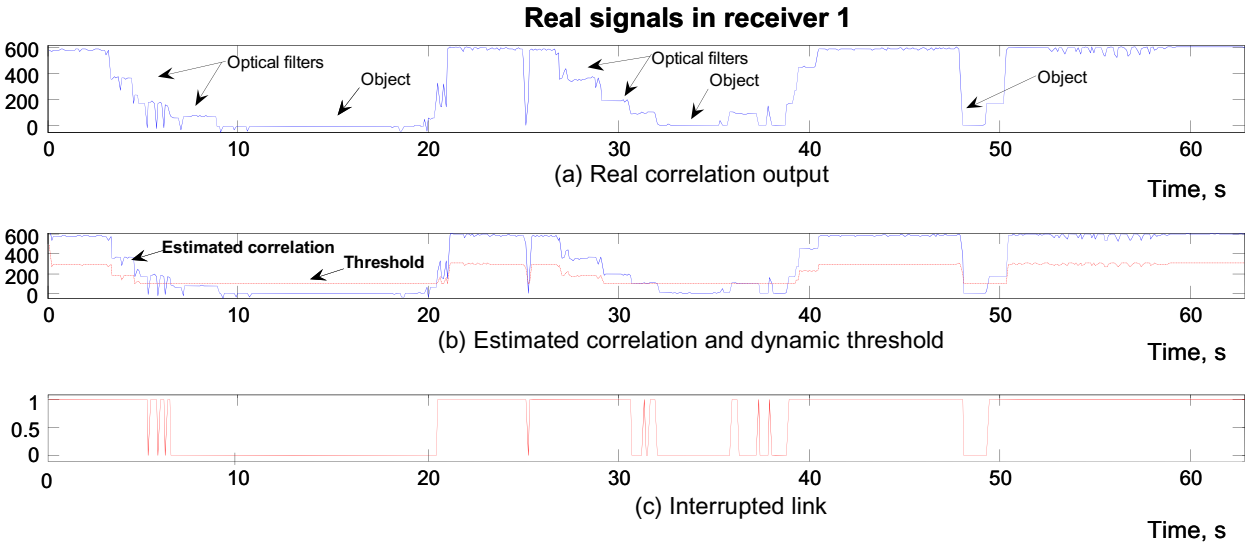

Fig. 25. Real signals in an IR receiver when high attenuation exists: (a) real correlation output; (b) estimated correlation output and dynamic threshold; and (c) state of the link.

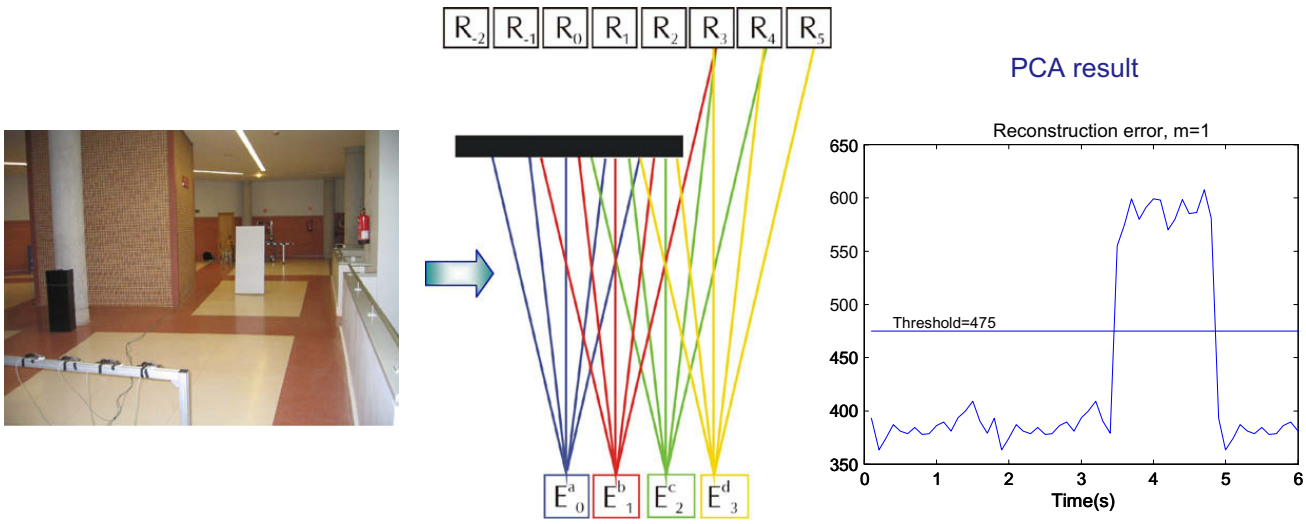

Fig. 26. Reconstruction error when an object larger than 0.5 m of side exists.

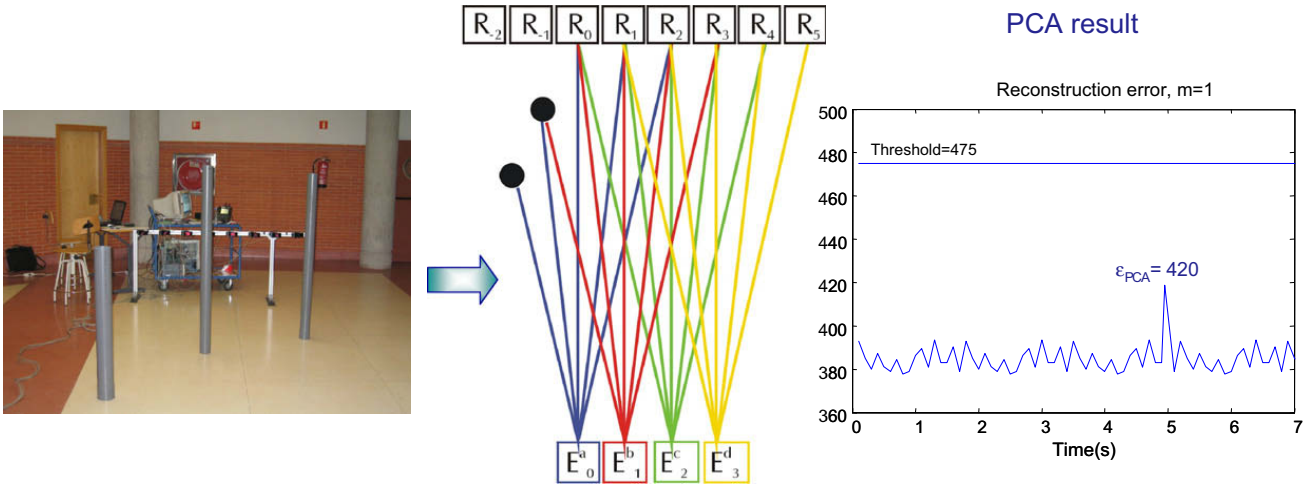

Fig. 27. Reconstruction error when there are random interruptions of the links.

obtained as was described in Section 5, with the necessary adaptation to the dimensions of the barrier. Fig. 26 shows a situation where an obstacle larger than 0.5 m of side is in the detection area. It interrupts several consecutive links. In this case the reconstruction error is higher than the threshold. This information should generate an alarm for the existence of dangerous objects. Conversely, Fig. 27 shows a situation where several links are randomly interrupted by small objects. As the reconstruction error is lower than the threshold, alarms should not be generated. In both situations, only one eigenvector has been used in the final transformation, what implies a high reduction in redundant information and a reduced process time.

8. Conclusions

A proposal for a system for obstacle detection on railways has been presented. The sensory system is based on two infrared barriers, one with the emitters and the other with the receivers, placed on opposing sides of the railway as required by Spanish Railway Regulations. The existence of obstacles is detected by the link interruption between both barriers.

The proposed structure of the sensory system improves others that use the same technique to detect obstacles on the railway. With the proposed geometrical distribution of the sensors, the obstacles can be detected with a high reliability, and their longitudinal and transverse positions can be obtained. Furthermore, the system can distinguish the existence of obstacles from a damaged sensor.

As results show, the encoding technique based on MO sets of sequences provides a high immunity against the infrared channel degradation.

Typical false alarms have been analysed, and several solutions have been proposed to reduce such false alarms based on Kalman and *minimax* filtering (H_∞ filter). Where there is some previous knowledge of the noise statistical, Kalman Filter works properly. Better results have been obtained with *minimax* filtering when there is no information about the channel noise model and when the worst case of estimation error needs to be minimized in order to increase railway safety.

Since there is a big amount of correlated information in the sensory system, Principal Component Analysis has been proposed to reduce such information before a decision is taken. Results show that this technique is suitable to validate the obstacle detection, and it increases the reliability of the system. It permits to distinguish situations of existence of dangerous objects (larger than 0.5 m of side) from those that are not.

PCA works well for the scenarios that have been used in the *off-line* phase (training process), and takes into account all the measurements. Although optimal filtering is much more robust, it only performs on single receivers. The latter gives additional information about how good the estimation is.

Though simulations show the feasibility of the proposed solutions, a complete prototype has been implemented to perform real tests, and the experimental results have verified the validity of the described algorithms.

Acknowledgments

The work described in this paper has been possible by funding from Spanish Ministry of Education and Science (RESELAI project, ref. TIN2006-14896-C02-01); the Spanish Ministry of Public Works (VIATOR project, ref. 70025/T05), and the University of Alcalá-Community of Madrid (MEFASRET project, ref. CCG06-UAH/DPI-0748).

References

Álvarez, F.J., Ureña, J., Mazo, M., Hernández, A., García, J.J., Jiménez, J.A., 2004. Efficient generator and pulse compressor for complementary sets of four sequences. IEE Electronics Letters 40 (11), 703–704.

Arai, M., 2003. Railway safety for the 21st century. Japan Railway & Transport Review 36.

Bloom, S., Korevaar, E., Schuster, J., Willebrand, H., 2003. Understanding the performance of free-space optics [Invited]. Journal of Optical Networking 2 (6), 178–200.

Bon, P., Cassir, C., 2004. Overview of national and european projects european commission (railway safety management). In: Fifth Framework Programme SAMNET Thematic Network, February 12th, 2004.

Díaz, M.J., García, J.J., Hernández, A., Losada, C., García, E. 2007. Advanced Multisensorial Barrier for Obstacle Detection. In: Proceedings of 2007 IEEE International Symposium on Intelligent Signal Processing, WISP2007. October 2007.

Dutton, K., Thompson, S., Barraclough, B., 1997. The Art of Control Engineering. Addison-Wesley.

European Directive, 2001. 2001/12/CE del Parlamento Europeo y del Congreso, de 26 de Febrero de 2001, por la que se modifica la Directiva 91/440/CEE sobre el Desarrollo de los Ferrocarriles Comunitarios, Diario Oficial de las Comunidades Europeas, L 75 de 15 de Marzo de 2001, SIN 1012-9200 (Published in Spanish).

Fenner, D., 2002. Train Protection. IEE review September 2002.

García, J.J., Ureña, J., Hernández, Á., Mazo, M., García, J.C., Álvarez, F., Jiménez, J. A., Donato, P., Pérez, C., 2004. IR sensor array configuration and signal processing for detecting obstacles in railways. In: Third IEEE Sensor Array and Multichannel Signal Processing Workshop SAM'04.

Garcia, J., Losada, C., Espinosa, F., Ureña, J., Hernández, Á., Mazo, M., Jiménez, A., Bueno, E., De Marziani, C., Álvarez, F., 2005[a]. Dedicated Smart IR Barrier for Obstacle Detection in Railways. IEEE Industrial Electronics Society, IECON 2005.

García, J.J., Losada, C., Ureña, J., Mazo, M., Hernández, Á., Donato, P., Álvarez, F., 2005b. Software for obstacle detection on railways, based on optical tecnhiques. XII Seminario Anual de Automática, Electrónica Industrial e Instrumentación (SAAEI'05). Santander, Spain. (Published in Spanish).

García-Márquez, F.P., 2004. Desarrollo de nuevos algoritmos aplicados al mantenimiento predictivo óptimo centrado en la fiabilidad y la monitorización remota basada en la condición (RCM2)". Thesis Doctoral. (Published in Spanish).

GIF, 2001. Gestor de Infraestructuras Ferroviarias. Obstacle detection system on railway. Technical and functional requirements (Published in Spanish).

GIF, 2004. Gestor de Infraestructuras Ferroviarias. Functional description of the object fall detector based on infrared sensors. (Published in Spanish).

Kim, I., Stieger, R., Koontz, J.A., Moursund, C., Barclay, M., Adhikari, P., Schuster, J., Korevaar, E., Ruigrok, R., De Cusatis, C., 1998. Wireless optical transmission of fast ethernet, FDDI, ATM, and ESCON protocol data using the TerraLink laser communication system. Optical Engineering 37 (12).

Laseroptronix, 2005. <http://www.laseroptronix.com>.

M°M de Fomento, 2005. Spanish Ministry of Public Works. Información Estadística. <http://www.fomento.es>.

Reitman, J., 1993. Achieving employee safety – lessons from the railroad. IEEE Technology and Society Magazine.

REOST Project Description, 2004. <http://spt.dibe.unige.it/ISIP/reost/projectdescription.html>.

Shu-Ming, T., Bell, M.R., 2000. Asynchronous multicarrier DS-CDMA using mutually orthogonal complementary sets of sequences. IEEE Transactions on Communications 48 (1), 53–59.

Simon, D., 2000. From here to infinity. Embedded Programming Systems. July, 2000.

Simon, D., 2005. To game theory approach to constrained minimax state estimation. Report of the Department of Electrical Engineering, Cleveland State University. January, 2005.

Smartmicro, 2005. <http://www.smartmicro.de/>.

Sorhea, Intelligent perimeter protection, 2009. <http://www.sorhea.com>.

Tseng, C.C., Liu, C.L., 1972. Complementary sets of sequences. IEEE Transaction on Information Theory IT-18 (5), 644–652.

Turk, M., Pentland, A., 1991. Eigenfaces for recognition. Journal of Cognitive Neuroscience 3, 72–85.